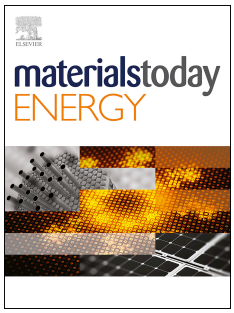

A wind driven rotational direct current triboelectric nanogenerator for self-powered inactivation of seawater microorganisms

Changxin Liu, Jianhao Liu, Jianhua Liu, Cong Zhao, Baichuan Shan, Nanxi Chen, Zhenghui Zhou, Chengfa Wang, Xinxiang Pan, Jianchun Mi, Minyi Xu

PII: S2468-6069(22)00049-1

DOI: https://doi.org/10.1016/j.mtener.2022.100991

Reference: MTENER 100991

To appear in: *Materials Today Energy*

Received Date: 11 November 2021

Revised Date: 10 March 2022

Accepted Date: 12 March 2022

Please cite this article as: C. Liu, J. Liu, J. Liu, C. Zhao, B. Shan, N. Chen, Z. Zhou, C. Wang, X. Pan, J. Mi, M. Xu, A wind driven rotational direct current triboelectric nanogenerator for self-powered inactivation of seawater microorganisms, *Materials Today Energy*, https://doi.org/10.1016/j.mtener.2022.100991.

CRediT author statement

Changxin Liu: Resources, Writing - Review & Editing, Supervision, Project administration, Funding acquisition

Jianhao Liu: Conceptualization, Methodology, Validation, Formal analysis, Investigation, Writing - Original Draft, Supervision

Jianhua Liu: Conceptualization, Validation, Investigation

Cong Zhao: Conceptualization, Validation, Investigation

Baichuan Shan: Investigation, Visualization

Nanxi Chen: Investigation, Visualization

Zhenghui Zhou: Visualization

Chengfa Wang: Writing - Review & Editing

Xinxiang Pan: Supervision, Project administration, Funding acquisition

Jianchun Mi: Writing - Review & Editing, Supervision

Minyi Xu: Writing - Review & Editing, Supervision, Funding acquisition

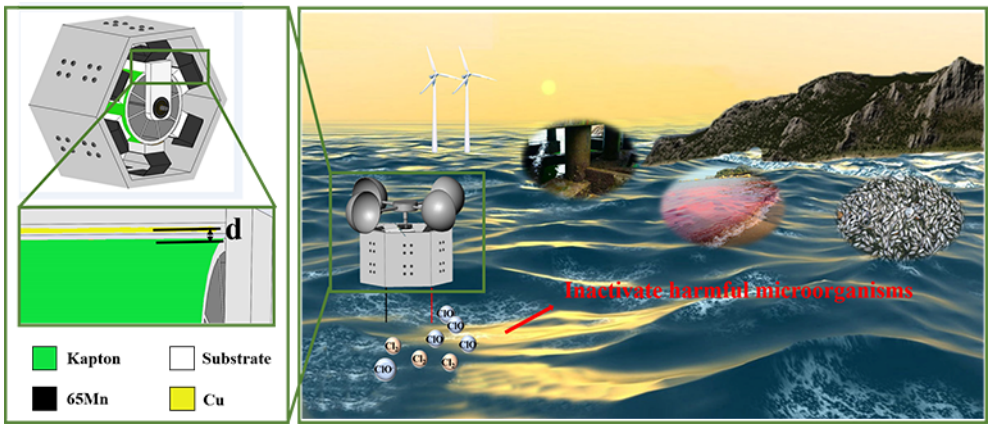

A wind driven rotational direct current triboelectric nanogenerator for self-powered inactivation of seawater microorganisms

Changxin Liu[1,2*], Jianhao Liu[1,2], Jianhua Liu[1], Cong Zhao[1,2], Baichuan Shan[1,2], Nanxi Chen[1,2], Zhenghui Zhou[1,2], Chengfa Wang[1], Xinxiang Pan[3], Jianchun Mi[4], Minyi Xu[1,2]

[1]Marine Engineering College, Dalian Maritime University, Dalian, 116026, China

[2]Dalian Key Lab of Marine Micro/Nano Energy and Self-powered Systems, Marine Engineering College, Dalian Maritime University, Dalian, China

[3]School of Electronics and Information technology, Guangdong Ocean University, Zhanjiang, 524088, China

[4]College of Engineering, Peking University, Beijing, 100871, China

*Address correspondence to liu_changxin@dlmu.edu.cn

Abstract:

While marine microorganisms may pollute water bodies and cause biofouling of marine facilities, they can be effectively inactivated by electrolysis. The present study develops a wind-driving rotating direct current triboelectric nanogenerator (R-DC-TENG) by coupling the triboelectrification and electrostatic breakdown for the self-powered electrolysis. Such a R-DC-TENG can convert the wind energy into DC electricity through wind cup without any rectifier device more efficiently than the traditional alternating current (AC) method. At the wind speed of 10 m/s, one R-DC-TENG device can generate the open-circuit voltage of 450 V, and the short-circuit current of 11 μA. The corresponding electrolysis can produce the chlorine of 0.8 mg/L, within 60 minutes, which is used to inactivate microalgae. Multiple devices can be connected in parallel to generate sufficient DC electricity for the electrolysis of seawater. It is anticipated that the R-DC-TENG will have a good application prospect in inactivating microorganisms near coasts or small islands and preventing marine microorganism pollution in shallow seawaters.

Key words: triboelectric nanogenerator, direct current, self-powered, inactivate marine microorganisms.

1. Introduction

Our exploration and development of the ocean discharge a plenty of N and P pollutants that leads to the proliferation of algae, thus affecting the marine environment seriously. The microalgae, protozoa or bacteria in the ocean proliferate or aggregate to a certain level under certain environmental conditions, it causes discoloration of water bodies or harming other organisms in the ocean, which is called red tide, see Figure 1. The formation of red tides not only competes with local species for limiting food resources and space resources, but also disrupts the local ecological balance, directly causing the degradation and even extinction of local species. In the marine environment, one of the main characteristics of the corrosion process of materials is the microbial corrosion caused by the biological activity of the seawater (Fig. 1). To prevent corrosions and red tides, marine microorganisms are necessary to be inactivated by using electrochemical technologies. The electrolysis of seawater is such a technology that generates the chlorine and hypochlorite to inactivate marine microorganisms. Nevertheless, the requirement of power grids and marine environments have limited the applications of conventional electrochemical methods.

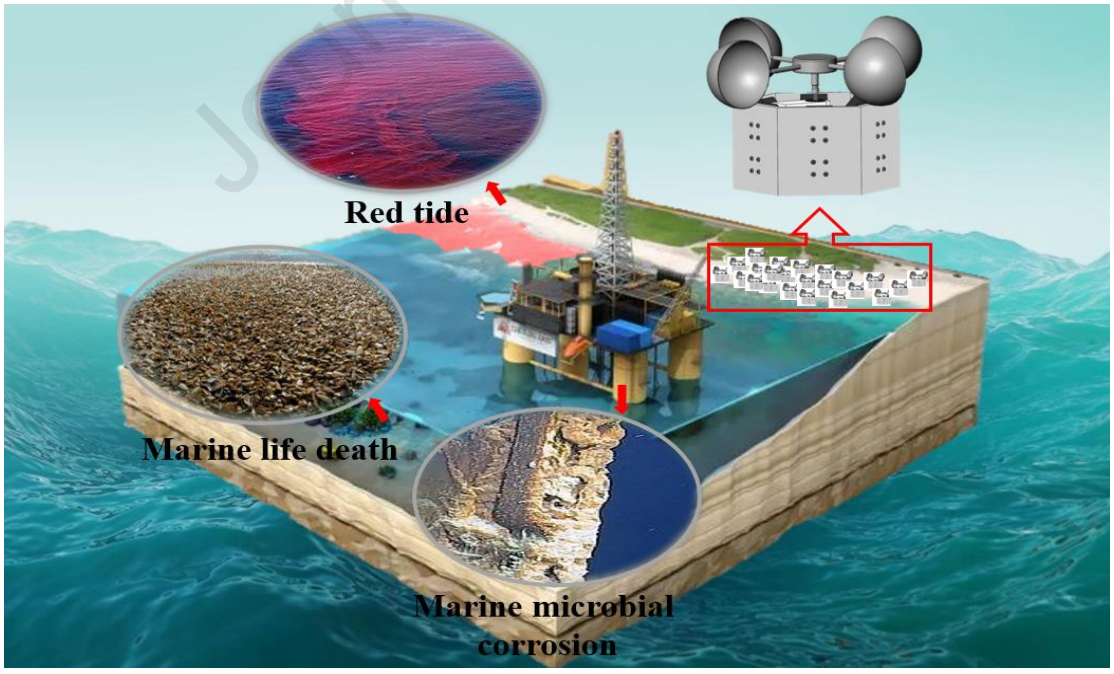

Figure 1. Possible application of the self-powered electrolysis by a wind-driving rotating direct current triboelectric nanogenerator (R-DC-TENG).

It is a green and effective method to collect the energy in the environment to electrolyze seawater and produce effective chlorine to inactivate harmful marine microorganisms. There are various forms of energy in nature, such as solar energy [1,2], wind energy [3,4], waste heat energy [5-7], etc. Collecting and converting those energies into electricity plays a key role in driving electronic devices and sensor networks in the Internet of Things (IoT) [8].

Triboelectric Nanogenerator (TENG) is an environmental energy harvesting technology that couples the triboelectrification and electrostatic induction. It has the advantages of simple structure, light weight, wide selection of materials, low cost, and high-efficiency output, even under low-frequency mechanical movements [9-17]. The output of the TENG based on the triboelectrification and electrostatic induction is alternating current (AC). Therefore, a rectifier is necessary to obtain a direct current (DC) output for electrolysis.

Recently, sliding Schottky nanocontact technique has achieved continuous DC output [18]. However, due to the relatively low voltage, it is not possible to supply power to electronic devices directly. To address this issue, a DC triboelectric nanogenerator (DC-TENG) has been developed based on the coupling of the triboelectrification effect and electrostatic breakdown. The electrostatic breakdown is usually considered as a negative effect of the TENG. It greatly limits the maximum charge density of TENG retaining, which leads to the performance of the TENG suddenly drops intermittently. Through the design of the structure, the electrostatic breakdown can be utilized cleverly to make a DC-TENG to obtain a DC output, realizing a direct power supply for small electronic devices [19-23]. Luo et al. [24] designed a contact separation type DC-TENG. It can directly charge the energy storage unit and drive electronic equipment without bridge rectifiers. It can be designed into a flexible power generation device with its simple structure, which expanded its application in flexible electronics and flexible self-charging power supply systems. Chen et al. [25] designed a DC fabric TENG, it can use the annoying electrostatic breakdown phenomenon on clothing to collect biological movement energy.

The present study develops a rotating DC triboelectric nanogenerator (R-DC-TENG) specifically for the self-powered electrolysis of seawater that can inactivate marine microorganisms (see Fig. 1). The wind cup collects wind energy and drives the rotor to rotate. A friction layer with strong electronegativity is attached to the surface of the rotor. The friction layer on the stator and the friction electrode have friction generating charge transfer and accumulation. When reaching the critical value of electrostatic breakdown, the charge will transfer back to the original electrode through the ionized air channel generated by electrostatic breakdown, forming a closed loop. In this way, a pulsed DC output can be generated. The parallel connection of multiple R-DC-TENGs can be used to form DC power arrays, collecting wind energy to electrolyze seawater for production of chlorine, thus incapacitating microorganisms. This research proposes the DC-TENG electrolyzing seawater can be flexibly distributed without environmental restrictions. Accordingly, it is believed that the present method can help to relieve marine microbial corrosion on offshore platforms and red tides near the coast.

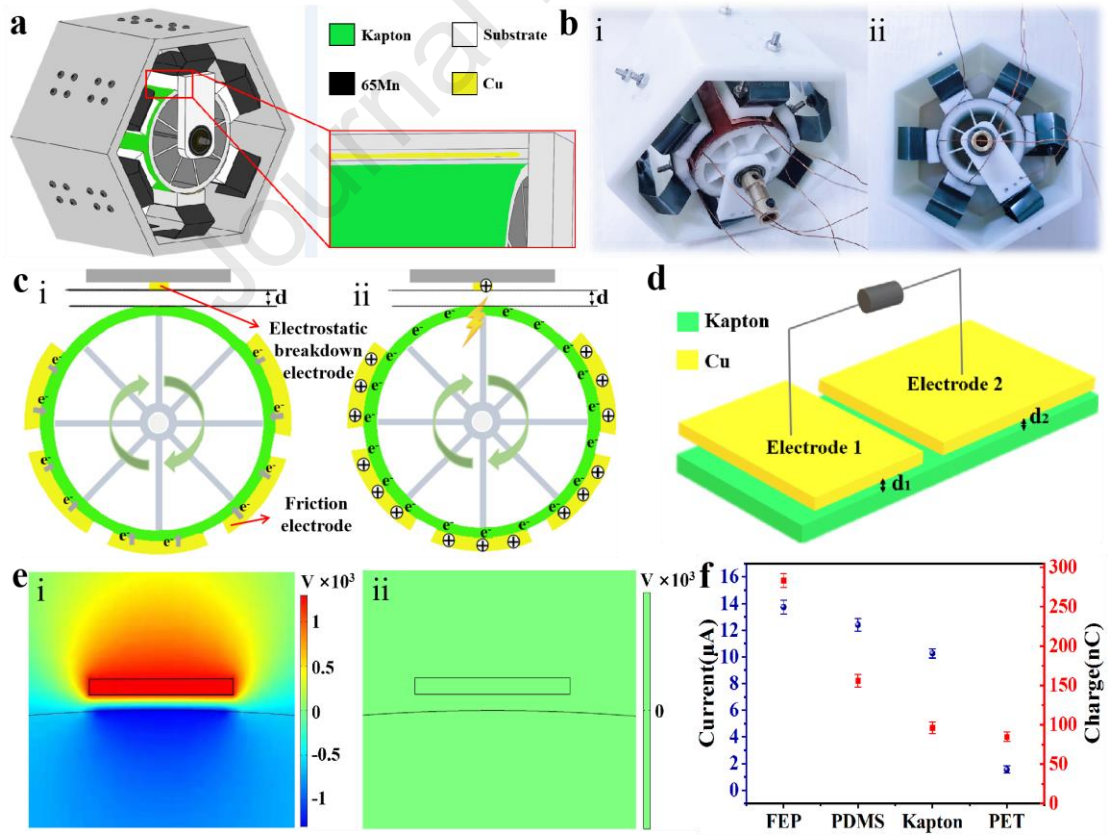

Figure 2. Structure and operating principle of R-DC-TENG. (a) Schematic of R-DC-

TENG model; (b) photographs of real R-DC-TENG; (c) operating principle of R-DC-TENG: (i) charge transfer process in the initial state and (ii) electrostatic breakdown occurring; (d) a test circuit; (e) results of COMSOL simulation (i) before and (ii) after the electrostatic breakdown; (f) comparison of DC-TENG for different triboelectric materials.

2. Results and Discussion

2.1 Structure and working principle of the R-DC-TENG

The basic structure of R-DC-TENG is shown in Figure 2a. A polyimide (Kapton) friction layer with high electronegativity is attached to the surface of a rotor, which rotates and rubs with the friction electrode (FE) fixed on the tolerance compensation device. FE here is made of copper (Cu) while all of them are connected. The main function of FE is to rub against the friction layer to cause charge transfer. The function of the tolerance compensation device is to make the friction layer and the FE contact close, keeping the rotor and FE of the semicircular structure to be coaxial, and the device to run smoothly. The electrostatic breakdown electrode (EBE) is also made of copper, it fixed on the base which is connected to the shaft through the bearing. The main function of EBE is to collect charge. There is a small distance between the EBE and the friction layer. The tiny distance is an important parameter of R-DC-TENG. Figure 2b displays two photographs of the real R-DC-TENG device.

When the rotor rotates, the EBE will remain stationary. In this process, since the electronegativity of copper electrode is lower than that of Kapton [26], electrons will transfer to the Kapton surface. Since Kapton is an insulator and has good wear resistance, electrons will stay on its surface for a long time. In this way, a higher electrostatic field will be established between the friction layer and the EBE. When the dielectric strength between the friction layer and the EBE exceeds the dielectric strength of air (≈ 3 kV/mm according to Paschen's law), a part of the air between the friction layer and the EBE is ionized to produce ionized air channels. The charges on the friction layer will transfer to the EBE. Thus, electrostatic breakdown occurs, balancing the

potential difference. The working principle is shown in Figure 2c.

As for the electron flow direction, when the friction layer on the rotor surface contacts and rubs with the FEs, the electrons on the FEs will transfer to the friction layer of Kapton. With the continuous transfer and accumulation of electrons, the electrostatic field between the friction layer and the EBE gradually increases. After the electrostatic breakdown occurring, the electrons will transfer from the friction layer to the EBE, and finally return to the FEs through the external circuit. So, the moving direction of electrons is unidirectional. The rotor keeps rotating under the action of external force, there will be pulsed DC output continuously. The R-DC-TENG can be simplified as two plate capacitors (Figure 2d), the specific theoretical derivation can refer to the supporting information, see S1. The effective working area of the R-DC-TENG is 50×75 mm^2. Figure 2e shows the simulation results of potential distribution before and after the electrostatic breakdown. The stronger electronegative friction materials such as polydimethylsiloxane (PDMS), polyethylene terephthalate (PET) and fluorinated ethylene propylene (FEP) are utilized to replace polyimide (Kapton) for comparison. Figure 2f compares the output currents and charges of DC-TENG with these four triboelectric materials under the same conditions. It is clearly shown that the order of FEP > PDMS > Kapton > PET is for both the current and charge. This order is consistent with the recognized friction sequence table [27]. Although Kapton is ranked as the third in the power generation performance, it is still utilized as the triboelectric material in this study since it has a good wear resistance.

2.2 Performance of the R-DC-TENG

Figure 3 shows the structure and performance of the present R-DC-TENG versus a rotating AC triboelectric nanogenerator (R-AC-TENG). The two structures use the same materials (Cu and Kapton) for their electrodes and friction layers, and also the identical area for their electrode surfaces. The two structures are schematically shown in Figures 3a and 3d, respectively. Figure S1 illustrates the working principle of R-AC-TENG.

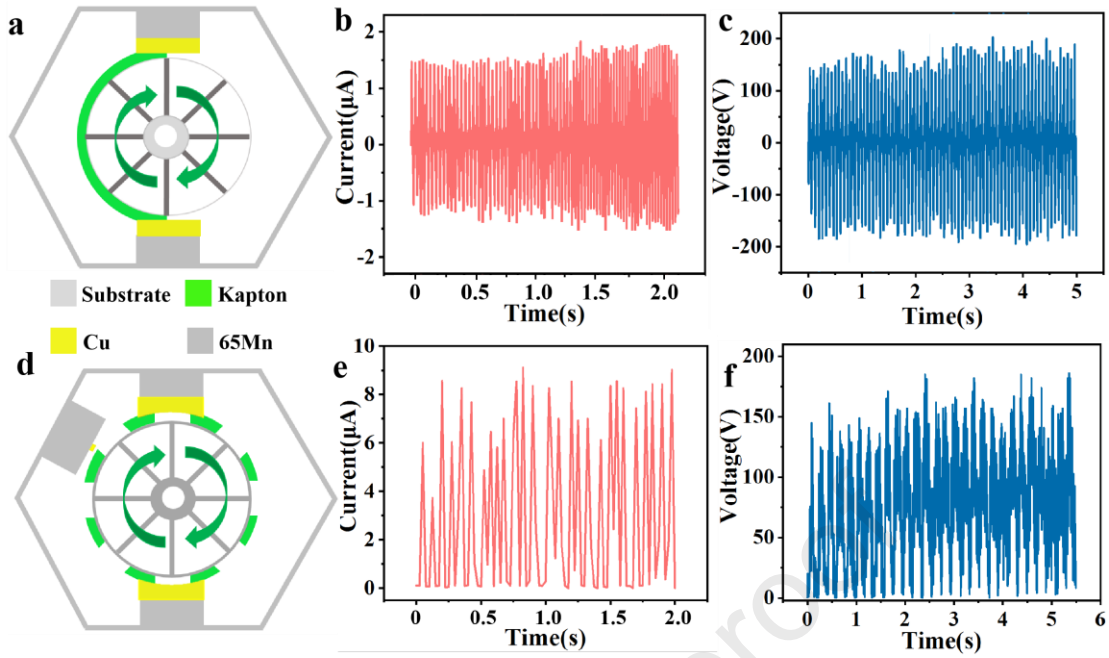

Figure 3. Performance comparison between R-AC-TENG and R-DC-TENG for the same wind speed of 10 m/s. (a-c) R-AC-TENG: (a) device structure, (b) output short-circuit current, and (c) output open-circuit voltage; (d-f) R-DC-TENG: (d) device structure, (e) output short-circuit current, and (f) output open-circuit voltage.

Although the two devices are similar in structure, their working principles are different. The working principle of R-AC-TENG is based on triboelectrification and electrostatic induction, while the R-DC-TENG works on the basis of triboelectric effect and electrostatic breakdown. The R-DC-TENG can produce continuous DC output without connecting a rectifier unit. Figures 3b and 3e present the short-circuit currents (I_{sc}) of the two devices, respectively. At the same wind speed of 10 m/s, I_{sc} is much higher from R-DC-TENG than that from the R-AC-TENG. The reason follows. If the contact areas between the friction electrode and the friction layer are the same, the two TENG structures should have the same number of electrons transferring from the electrode to the friction layer per unit time. The R-AC-TENG generates an alternating signal directly through electrostatic induction, while the charge on the R-DC-TENG friction layer needs to accumulate to a certain value before a DC signal is emitted. So, the instantaneous current of R-DC-TENG is greater than that of R-AC-TENG. The current is an important parameter for electrolysis of seawater. Comparing with AC-

TENG, DC-TENG has a good prospect in electrolysis of seawater. Figures 3c and 3f represent the open-circuit voltages (V_{oc}) of R-AC-TENG and R-DC-TENG, respectively. It can be seen that the voltage values generated by these two devices with different structures are not much different. Since the materials employed in the two structures are the same, the charge density of the materials is the same, and the contact area between the electrode and the friction layer is also the same. The R-DC-TENG directly outputs the DC voltage without connecting any rectifier device, so it can be directly utilized as an energy supply unit and has broad application prospects.

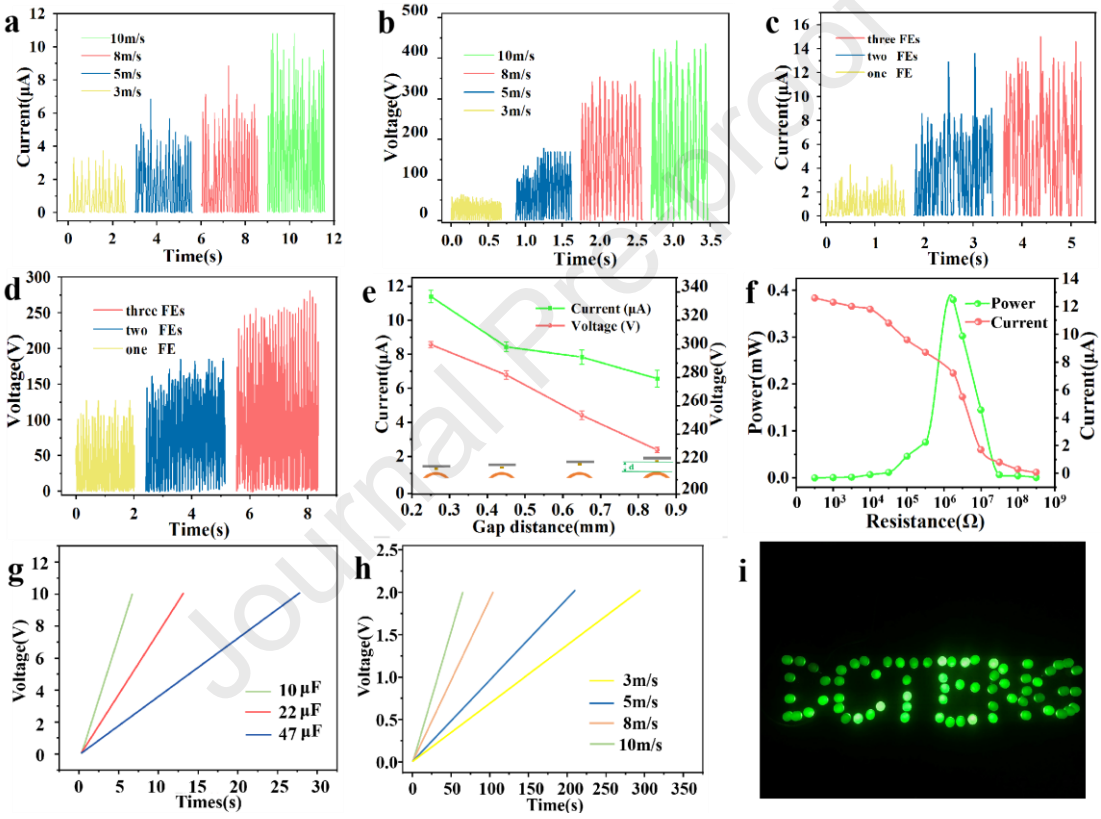

Figure 4. Output performance of the R-DC-TENG under various conditions. Different wind speeds: (a) short-circuit current and (b) open-circuit voltage; different friction-electrode number: (c) short-circuit current and (d) open-circuit voltage; (e) averaging peak values of I_{sc} and V_{oc} under different d; (f) peak short-circuit current and peak power versus load resistance; (g) output voltages for different charged capacitances at the wind speed of 10 m/s; (h) output voltages of a capacitor (470 μF) at different wind speeds; (i) R-DC-TENG lighting up small LED lights.

Figure 4 illustrates the output performance of the R-DC-TENG under various conditions. The measured signals of I_{sc} and V_{oc} of R-DC-TENG are shown, respectively, in Figures 4a and 4b for the wind speed of U = 3-10 m/s. Note that an electric fan is used to generate airflow or wind at different preset speeds in the experiments; the wind cup collects the wind energy and drives the rotor to rotate. Evidently, as U rises gradually, the peaks of V_{oc} increase approximately from 60 V to 450 V, while those of I_{sc} increase from 3 μA to 11 μA. The main reason is that the increase of the rotor speed caused by raising U speeds up the charge transfer between the friction layer and the FEs, i.e., rises the number of charges transferring per unit time, consequently increasing the current. Also, it is observed that both I_{sc} and V_{oc} are positively correlated with the speed of rotor. The theoretical derivation of the result can be seen from Supporting information for Note S2.

We have experimentally examined the effect of the effective contact area (A) between the FE and the friction layer on the power generation performance of R-DC-TENG through changing A by varying the FE number (N). Figures 4c and 4d present the output signals of I_{sc} and V_{oc} versus N. It is obvious that, as N grows, A increases, the V_{oc} and I_{sc} rise accordingly. This is because the number of charges transferring per unit time increases as A increases. The specific theoretical derivation of the result can be seen from Note S3 of Supporting information.

In addition, the distance (d) between the EBE and the friction layer is a key parameter that affects the power generation performance of R-DC-TENG. Figure 4e shows I_{sc} and V_{oc} for different d. Obviously, I_{sc} and V_{oc} decrease as d increases. This result can be explained here. As d is increased, the strength of the electric field reduces, because the number of charges from air break-down decreases. Therefore, reducing d is an effective way to improve the power generation of R-DC-TENG.

The external load of R-DC-TENG has a great influence on the power generation. In the experiments, I_{sc} and the peak power at different resistance values are shown in Figure 4f. The output current was measured with various resistors as the external load. The peak power of the device is calculated by $P = I^2R$, where I is the output peak current

across the load, R is the load resistance. It is obvious that I_{sc} decreases as the external load increases, the peak power first increases and then decreases. So, it can be concluded that the matching impedance of R-DC-TENG is about 1 MΩ.

In the experiments, a 470 μF capacitor is charged by the R-DC-TENG for the wind speed of U = 3-10 m/s in order to prove the DC output characteristics. Figure 4g presents the voltage charging curve. It is obvious that, as the wind speed grows, the charging rate increases. It only takes 50 s in time to charge to 2 V for the wind speed of U = 10 m/s. Figure 4h shows that the R-DC-TENG charges 10 μF, 22 μF and 47 μF capacitors respectively under the wind speed of U = 10 m/s. It takes only 5 s for the 10 μF capacitor to charge to 10 V, which fully reflects the good DC output characteristics of the R-DC-TENG. Figure 4i shows that the R-DC-TENG lights up 67 small LED lights.

2.3 Application of R-DC-TENG

Marine microorganisms are harmful and should be well treated to protect the ecotopia. Relying on the R-DC-TENG generating DC electricity, the electrolysis can produce chlorine and hypochlorite to inactivate microorganisms in seawater near coasts or small islands, so preventing marine microbial pollution in shallow waters. Figure 5a schematically shows the seawater electrolysis system. The rotor of R-DC-TENG can be driven to rotate by airflow through the wind cup, which collect wind energy from the environment. Multiple R-DC-TENGs can be connected in parallel to form arrays to constitute a self-powered electrolytic seawater system. Figure 5a (i) also displays the electrolysis principle. Since the seawater contains a plenty of chloride ions, its number accounts for about 55% of the total number of ions [28].

The electrolytic ion reactions are as follows [29]:

$$\text{Anode：} 2Cl^- \rightarrow Cl_2+2e \quad (1)$$

$$\text{Cathode：} 2H_2O+2e \rightarrow 2OH^-+H_2 \quad (2)$$

Since chlorine gas is easily soluble in water, it immediately reacts twice in the solution, i.e.,

$$Cl_2+2OH^- \rightarrow ClO^-+Cl^-+H_2O\ . \quad (3)$$

The total response of the above three reactions can be written as

$$NaCl+H_2O=NaClO+H_2\ . \quad (4)$$

ClO^- and Cl_2 produced in reactions (1) and (3) are all called available chlorine (a parameter indicating how much effective disinfection ingredients are contained in the chloride). Available chlorine can destroy the cell structure of marine microorganisms. The available chlorine obtained by electrolysis of seawater inactivates microorganisms in seawater. Figure 5a (ii) shows the experimental setup for electrolysis.

Figure 5b shows the variation of the available chlorine concentration against different time spans of electrolysis by utilizing two different structures of TENG, i.e., AC-TENG and DC-TENG, under the wind speed of U = 10 m/s. Evidently, for both TENG structures, the concentration increases approximately linearly as the electrolysis time increases. However, it is very important to note that the concentration of available chlorine in seawater generated by R-DC-TENG is substantially higher than (nearly as twice as) that of R-AC-TENG at any time span of electrolysis within 60 minutes. In other words, the efficiency of R-DC-TENG electrolyzing seawater to produce available chlorine is much higher than R-AC-TENG. This fact is also demonstrated in the following comparison between practical applications of inactivating marine microorganisms by the structures.

The realization of electrolysis can be determined by observing bubbles on the electrode surface or not. A series of experiments are conducted to validate whether R-DC-TENG can effectively act as an electric source to electrolyze seawater. The non-electrolyzed and electrolyzed seawaters in test cups are compared in Figure 5c. Evidently, after electrolyzing for 20 minutes, bubbles are clearly seen to occur on the electrode surface. This indicates that the present R-DC-TENG supplies electricity for the electrolysis of seawater. Hence, the R-DC-TENG can be utilized as an effective power source to electrolyze.

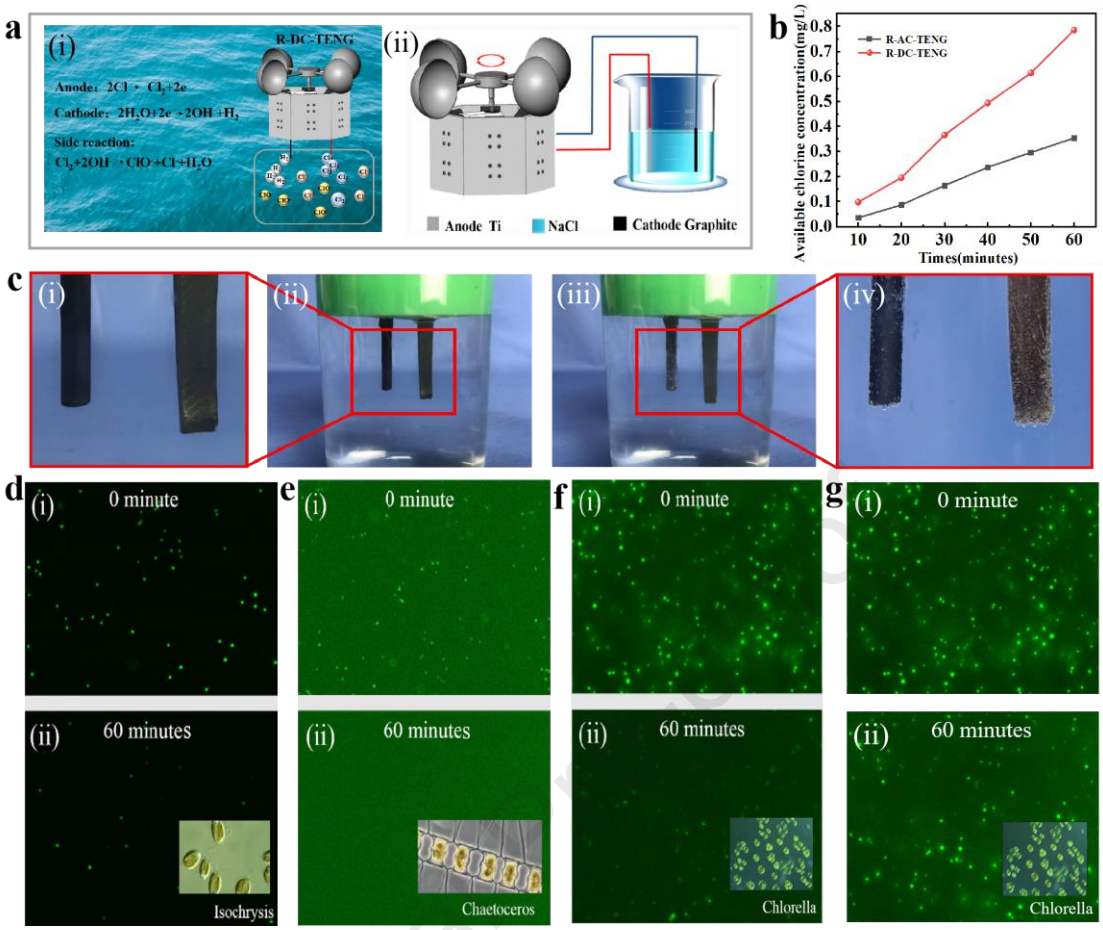

Figure 5. Validation of R-DC-TENG for electrolysis inactivating marine microorganisms. (a) Seawater electrolysis system & principle: (i) principle of electrolysis of sea water; (ii) experimental setup for electrolysis; (b) chlorine concentration versus electrolysis time; (c) comparison between (i, ii) non-electrolysis and (iii, iv) electrolysis for 20 minutes; (d-f) inactivating microorganisms using R-DC-TENG: comparisons between (i) non-electrolysis and (ii) electrolysis for 60 minutes for the activities of (d) isochrysis, (e) chaetoceros and (f) chlorella; (g) inactivating chlorella using R-AC-TENG to electrolyze seawater: (i) non-electrolysis and (ii) electrolysis for 60 minutes.

Now let us examine the inactivation of microalgae by the electrolysis of seawater due to the R-DC-TENG. In our experiments, three different microalgae at the same volume of 60 mL are mixed with seawaters, and then the mixture is electrolyzed. For 6 hours of processing, laser-induced fluorescence technology is utilized to inspect the

activity change of culture solution [30]. Figures 5d-5f compare experimental results of three different microorganisms inactivated by electrolysis of 60 minutes versus non-electrolysis or electrolysis of 0 minute. More comparisons are also made in Figures S2-S5 for electrolysis of 10-60 minutes versus the non-electrolyzed cases. Importantly, Figures 5g and S2 show the effect of inactivating chlorella using R-AC-TENG of similar structure to electrolyze same volume of seawater. As seen in Figures 5d-5f, after 60 minutes of electrolysis, the amounts of isochrysis, chaetoceros and chlorella reduce substantially, hence validating the inactivation by electrolysis. Besides, Figures S3-S5 demonstrate that the inactivation takes effective in about 20, 45 and 60 minutes for chaetoceros, isochrysis and chlorella, respectively. This suggests that, in general, different microorganism requires different chlorine concentration or time span of electrolysis for their inactivation.

In order to compare the effects of R-DC-TENG and R-AC-TENG in inactivating chlorella, an experimental study to electrolyze seawater is carried out. The volume and concentration of the two seawater samples are the same. After mixing the seawater samples electrolyzed for different times with the culture solution of chlorella, the activity of chlorella is observed. The electrolysis of 60 minutes by the R-DC-TENG can inactivate chlorella very effectively (see Figure 5f). However, the inactivation by the R-AC-TENG is not so good, as shown in Figures 5g and S2. This clearly demonstrates a better performance of the R-DC-TENG than that of the R-AC-TENG, due to the higher efficiency of the former structure for the available chlorine as shown in Figure 5b.

3. Conclusion

This study has proposed a R-DC-TENG based on coupling the triboelectrification effect and electrostatic breakdown effect for electrolysis to solve the marine environmental problems caused by red tides near the coast and marine biofouling. When the friction layer on the rotor surface contacts and rubs with the friction electrodes (FEs), the electrons on the FEs will transfer to the friction layer Kapton. With

the continuous transfer and accumulation of electrons, the electrostatic field between the friction layer and the electrostatic breakdown electrode (EBE) gradually increases. As the electrostatic breakdown occurs, electrons will transfer from the friction layer to the EBE and finally return to the FEs through the external circuit. The R-DC-TENG system can collect environmental energy and convert it into electricity more efficiently than the traditional R-AC-TENG system. It has the advantage of direct DC output without a rectifier device over the AC output, and can be placed near coasts or offshore platforms. Above all, the R-DC-TENG system can be effectively utilized to supply electricity for electrolyzing seawater to produce available chlorine and then for inactivating marine microorganisms.

The device can generate electricity at various wind speeds. At the wind speed of 10 m/s, the open-circuit voltage can reach 450 V in peak, the short-circuit current can reach 11 μA in peak, and the matched impedance is about 1 MΩ. Increasing the FE area or reducing the distance between the friction layer and the EBE can improve the power generation performance of R-DC-TENG. When the R-DC-TENG is employed to electrolyze seawater, the available chlorine of 0.8 mg/L is produced within 60 minutes. Multiple R-DC-TENGs are connected in parallel to form a DC power supply array. The generated direct current is utilized to electrolyze seawater near offshore platforms or the coast to form a self-powered electrolysis system, inactivating microorganisms in seawater, which has a good application prospect in inactivating microbes in seawater near coasts or small islands and preventing marine microbial pollution in shallow seawaters.

4. Methods

4.1 Fabrication of R-DC-TENG

R-DC-TENG is composed of a rotor with a friction layer (Kapton) on the surface, electrostatic breakdown electrode(EBE), electrostatic breakdown electrode base, friction electrode(FE), friction electrode base, a tolerance compensation structure and a support shell.

The materials of the EBE and the FEs are both metallic copper, and the size of the EBE is 50 mm (length) × 2 mm (width) × 0.25 mm (thickness). The size of the FE is 50 mm (length) × 16 mm (width) × 0.25 mm (thickness).

The rotor is made of PLA material and produced by a 3D printer. The outer diameter of the rotor is 50 mm, the diameter of the shaft is 3 mm, and the bearings are self-aligning ball bearings. The Kapton film has a thickness of 0.05 mm, it is stuck on the surface of the rotor. During the rotation, the power is driven by a fan (130FLJ2).

The EBE base and FEs base are also printed with PLA, they are produced by a 3D printer. The EBE base and the bearing can be disassembled, so that it is convenient to add insulating material on the base to change the distance between the EBE and the friction layer. The specific size of the EBE base is 50 mm (length) × 16 mm (width) × 5 mm (thickness). The upper surface of the FEs have a certain arc, and the radius of curvature is 25 mm. The main purpose is to have a closer contact between the FEs and the friction layer. Its specific size is 50 mm×16 mm×5 mm.

The tolerance compensation structure is mainly to make the FEs and the Kapton friction layer contact more closely, at the same time, it can ensure that the rotor and the FEs base maintain the same concentricity. The material is 65Mn spring steel, which has been quenched and heat treated to have high elasticity. Its thickness is 0.15 mm, width is 16 mm, it is folded into a non-equilateral hexagon, and the two opposite sides can be compressed up and down, so that it has good elasticity.

4.2 Measurement of R-DC-TENG

A Keithley 6517B electrometer was used to measure the short-circuit current and the amount of charge transfer for DC-TENG. The HVP-40 type high voltage attenuation rod (attenuation ratio 1000:1) is connected to the Keithley 6517B electrometer to measure the open circuit voltage of the R-DC-TENG. During the experiment, the wind speed is measured by an anemometer (Testo 410)

The available chlorine concentration is measured by DPD (N, N-diethyl-1,4 -phenylenediamine sulfate) colorimetric method. The basic principle is that available chlorine in NaClO solution is at pH of 6.2-6.5. It reacts with DPD sulfate to form a red

compound. The absorbance of the red compound solution is measured by an ultraviolet-visible spectrophotometer (UV1800, Shimadzu, Japan) at a wavelength of 515 nm. The concentration of available chlorine in the solution can be obtained by comparing with the standard curve.

The detection of algae activity in seawater mainly utilizes laser-induced fluorescence detection technology. When certain substances are irradiated by light of a specific wavelength, they will be excited to produce visible light of certain color. Once the irradiation is stopped, the visible light generated by this excitation will disappear. The microalgae in seawater contains chlorophyll, and chlorophyll has a fluorescence effect. However, inactivated microalgae have no biological enzyme in the microalgae, so the reacts with FDA generating fluorescein cannot react. When the microalgae is illuminated by an external light source, the fluorescent signal cannot be detected. The microalgae activity was observed by using an inverted fluorescence microscope (Ti-e, Nikon, Japan).

The process of microalgae cultivation is as follows, the filtered natural seawater is put into a 250 mL Erlenmeyer flask. The salinity is diluted with pure water to 30%. After high temperature disinfection, the solution is cooled at room temperature to make a seawater medium. The microalgae is inoculated into the culture medium and placed in a light medium with light intensity of 3100 cd/m^2 and temperature of 23 °C. The Erlenmeyer flask is shaken every eight hours, paying close attention to the growth of the microalgae with a microscope.

Acknowledgements

This work was supported by the Fundamental Research Funds for the National Key R & D Project from Minister of Science and Technology (2021YFA1201604), the Fundamental Research Funds for the Central Universities (Grants 3132019330), the National Natural Science Foundation of China (Grant Nos. 51779024, 51879022, 51979045, 51906029), Innovation Group Project of Southern Marine Science and Engineering Guangdong Laboratory (Zhuhai) (No.311021013), Natural Science

Foundation of Liaoning Province of China (2020MS130).

ORCID

Changxin Liu http://orcid.org/0000-0002-4748-1265

REFERENCES

[1] T.T. Wu, G.Q. Deng, C. Zhen, Metal oxide mesocrystals and mesoporous single crystals: synthesis, properties and applications in solar energy conversion, J. Mater. Sci. Technol. 73 (2021) 9-22. https://doi.org/10.1016/j.jmst.2020.09.025.

[2] M.R. Darwesh, M.S. Ghoname, Experimental studies on the contribution of solar energy as a source for heating biogas digestion units, Energy Rep. 7 (2021) 1657-1671. https://doi.org/10.1016/j.egyr.2021.03.014.

[3] C.X. Liu, C. Zhao, J.H. Liu, J.Y. Wang, Y. Wang, Y.H. Fan, K.Y. Zhao, B.C. Shan, Z.Y. Qu, K.F. Ma, M.Y. Xu, X.X. Pan, Design and study of a combining energy harvesting system based on thermoelectric and flapping triboelectric nanogenerator, Intj Green Energy. 12 (2021) 1-7. https://doi.org/10.1080/15435075.2021.1904405.

[4] Y. Wang, J.Y. Wang, X. Xiao, S.Y. Wang, P.T. K, J.L. Dong, J.C. Mi, X.X. Pan, H.F. Wang, M.Y. Xu, Multi-functional wind barrier based on triboelectric nanogenerator for power generation, self-powered wind speed sensing and highly efficient windshield, Nano Energy. 73 (2020) 104736. https://doi.org/10.1016/j.nanoen.2020.104736.

[5] C.X. Liu, W.X. Ye, H.A Li, J.H. Liu, C. Zhao, Z.F. Mao, X.X. Pan, Experimental study on cascade utilization of ship's waste heat based on TEG‐ORC combined cycle, Int. J. Energ. Res. 45 (2021) 4184-4196. https://doi.org/10.1002/er.6083.

[6] W.X. Ye, C.X. Liu, J.H. Liu, H.B. Wang, S.J. Yang, X.X. Pan, Research on TEG–ORC Combined Bottom Cycle for Cascade Recovery from Various Vessel Waste heat Sources, Arab J Sci Eng. https://doi.org/10.1007/s13369-021-06050-3.

[7] C.X. Liu, J.H. Liu, W.X. Ye, H.A. Li, C. Zhao, H.B. Wang, M.Y. Xu, X.X. Pan, Study on a new cascade utilize method for ship waste heat based on TEG-ORC combined cycle, Environ Prog Sustain. 40 (2021) e13661.

http://doi.org/10.1002/ep.13661.

[8] Z.L. Wang, Entropy theory of distributed energy for internet of things, Nano Energy. 58 (2019) 669-672. http://doi.org/10.1016/j.nanoen.2019.02.012.

[9] J.H. Lee, R. Hinchet, S.K. Kim, S. Kim, Shape memory polymer-based self-healing triboelectric nanogenerator, Energ Environ Sci. 8 (2015) 3605-3613. https://doi.org/10.1039/c5ee02711j.

[10] X. Cao, Y. Jie, N. Wang, Z.L. Wang, Triboelectric nanogenerators driven self-powered electrochemical processes for energy and environmental science, Adv Energy Mater. 6 (2016) 1600665. https://doi.org/10.1002/aenm.201600665.

[11] M. Wu, Z. Gao, K. Yao, S. Hou, Y. Liu, D. Li, J. He, X. Huang, E. Song, J. Yu, X. Yu, Thin, soft, skin-integrated foam-based triboelectric nanogenerators for tactile sensing and energy harvesting, Mater Today Energy. 20 (2021) 100657. https://doi.org/10.1016/j.mtener.2021.100657.

[12] Z.H. Yuan, X.L. Wei, X. Jin, Y.G. Sun, Z.Y. Wu, Z.L. Wang, Magnetic energy harvesting of transmission lines by the swinging triboelectric nanogenerator, Mater Today Energy. 22 (2021) 100848. https://doi.org/10.1016/j.mtener.2021.100848.

[13] M. Sahu, S. Hajra, J. Bijelic, O.H. Dongik, H.J. Kim. Triple Perovskites Based Triboelectric Nanogenerator: A Facile Method of Energy Harvesting and Self-Powered Information Generator, Mater Today Energy. 20 (2021) 100639. https://doi.org/10.1016/j.mtener.2021.100639.

[14] X.Q. Zhang, M. Yu, Z. Ma, H. Ouyang, Y. Zou, S.L. Zhang, H.K. Niu, X.X Pan, M.Y. Xu, Z. Li, Z.L. Wang, Self‐Powered Distributed Water Level Sensors Based on Liquid-Solid Triboelectric Nanogenerators for Ship Draft Detecting, Adv Funct Mater. 29 (2019) 1900327. https://doi.org/10.1002/adfm.201900327.

[15] H.Wang, F.Z. Qi, T.C. Zhao, J.L. Dong, S.Y. Wang, Y. Wang, X. Xiao, C.X. Liu, X.X. Pan, Y.P. Zhao, M.Y. Xu, Sandwich-like Triboelectric Nanogenerators Integrated Self-Powered Buoy for Navigation Safety, Nano Energy. 84 (2021) 105920. https://doi.org/10.1016/j.nanoen.2021.105920.

[16] H.F. Zhao, X. Xiu, P. Xu, T.C. Zhao, L.G. Song, X.X. Pan, J.C. Mi, M.Y. Xu, Z.L.

Wang, Dual-Tube Helmholtz Resonator-Based Triboelectric Nanogenerator for Highly Efficient Harvesting of Acoustic Energy, Adv Energy Mater. 9 (2019) 1902824. https://doi.org/10.1002/aenm.201902824.

[17] X.B. Gao, F.J. Xing, F. Guo, Y.H.Yang, Y.T. Hao, J. Chen, B.D. Chen, Z.L. Wang, A turbine disk-type triboelectric nanogenerator for wind energy harvesting and self-powered wildfire pre-warning, Mater Today Energy. 22 (2021) 100867. https://doi.org/10.1016/j.mtener.2021.100867.

[18] J. Liu, A. Goswami, K. Jiang,F. Khan, S. Kim, R. Mcgee, L. Zhi, Z. Hu, J. Lee, T. Thundat, Direct-current triboelectricity generation by a sliding Schottky nanocontact on MoS2 multilayers, Nat Nanotechnol. 13 (2018) 112-116. https://doi.org/10.1038/s41565-017-0019-5.

[19] D. Liu, X. Yin, H.Y. Guo, L.L. Zhou, X.Y. Li, C.L. Zhang, J. Wang, Z.L. Wang, A constant current triboelectric nanogenerator arising from electrostatic breakdown, Sci Adv. 5 (2019) eaav6437. https://doi.org/10.1126/sciadv.aav6437.

[20] H.J. Yoon, M.K. Kang, W.C. Seung, S.S. Kwak, J.Y. Kim, H.T. Kim, S.W. Kim, Microdischarge-Based Direct Current Triboelectric Nanogenerator via Accumulation of Triboelectric Charge in Atmospheric Condition, Adv Energy Mater. 10 (2020) 2000730. https://doi.org/10.1002/aenm.202000730.

[21] T.H. Kim, D.Y. Kim, J.S. Yun, B.S. Kim, S.H. Lee, D.G. Kim, S.G. Lee, Direct-Current Triboelectric Nanogenerator via Water Electrification and Phase Control, Nano Energy. 52 (2018) 95-104. https://doi.org/10.1016/j.nanoen.2018.07.048.

[22] J.Y. Wang, Z.Y. Wu, L. Pan, R.J. Gao, B.B. Zhang, L.J. Yang, H.Y. Guo, R.J. Liao, Z.L. Wang, Direct-Current Rotary-Tubular Triboelectric Nanogenerator Based on Liquid-Dielectrics Contact for Sustainably Energy Harvesting and Chemical Composition Analysis, ACS Nano. 13 (2019) 2587-2598. https://doi.org/10.1021/acsnano.8b09642.

[23] Y.D. Song, N. Wang, Y.H. Wang, R.Y. Zhang, H.K. Olin, Y. Yang, Direct Current Triboelectric Nanogenerators, Adv Energy Mater. 10 (2020) 2002756. https://doi.org/10.1002/aenm.202002756.

[24] J.J. Luo, X. Liang, W. Tang, T. Jiang, F.R. Fan, Y.K. Pang, L.B. Chen, Y. Zhang, Z.L. Wang, Direct−Current Triboelectric Nanogenerator Realized by Air Breakdown Induced Ionized Air Channel, Adv Energy Mater. 8 (2018) 1-8. https://doi.org/10.1002/aenm.201800889.

[25] C.Y. Chen, H.Y. Guo, L.J. Chen, Y.C. Wang, X.J. Pu, W.D. Yu, F.M. Wang, Z.Q. Du, Z.L. Wang, Direct Current Fabric Triboelectric Nanogenerator for Biomotion Energy Harvesting, ACS Nano. 14 (2020) 4585-4594. https://doi.org/10.1021/acsnano.0c00138.

[26] Y. Yang, G. Zhu, H. Zhang, J. Chen, X. Zhong, Z.H. Lin, Y. Su, P. Bai, X. Wen, Z.L. Wang. Triboelectric nanogenerator for harvesting wind energy and as self-power wind vector sensor system, ACS Nano, 7 (2013) 9461-9468. https://doi.org/10.1021/nn4043157.

[27] Z.L. Wang, L. Long, J. Chen, S.M. Niu, Y.L. Yu, Triboelectric Nanogenerators, Science Press, Beijing, 2017.

[28] T.Shimura, Y. Kon, Y.Sawaki, T.Hirata, J. Han, D. Shu, T. Komiya, In-situ analyses of phosphorus contents of carbonate minerals: Reconstruction of phosphorus contents of seawater from the Ediacaran to early Cambrian, Gondwana Res. 25 (2019) 1090-1107. https://doi.org/10.1016/j.gr.2013.08.001.

[29] K. Liu, X.L.Gao, Q.G. Xing, F.S. Chen, Adsorption kinetics of platinum group elements onto macromolecular organic matter in seawater, Acta Oceanol Sin. 38 (2019) 8-16. https://doi.org/10.1007/s13131-019-1433-3.

[30] Y.P. Yuan, A.R. Feng, Y.X. Song, Fully automatic single-cell electric manipulation technology on microfluidic chip, Science Technology and Engineering. 18 (2018) 78-82. https://doi.org/10.3969/j.issn.1671-1815.2018.12.012.

Supporting Information

A wind driven rotational direct current triboelectric nanogenerator for self-powered inactivation of seawater microorganisms

Changxin Liu[1,2*], Jianhao Liu[1,2], Jianhua Liu[1], Cong Zhao[1,2], Baichuan Shan[1,2], Nanxi Chen[1,2], Zhenghui Zhou[1,2], Chengfa Wang[1], Xinxiang Pan[3], Jianchun Mi[4], Minyi Xu[1,2]

[1]Marine Engineering College, Dalian Maritime University, Dalian, 116026, China

[2]Dalian Key Lab of Marine Micro/Nano Energy and Self-powered Systems, Marine Engineering College, Dalian Maritime University, Dalian, China

[3]School of Electronics and Information technology, Guangdong Ocean University, Zhanjiang, 524088, China

[4]College of Engineering, Peking University, Beijing, 100871, China

Files include:

Supplementary Materials and Methods

Note S1: R-DC-TENG equivalent capacitance theoretical model.

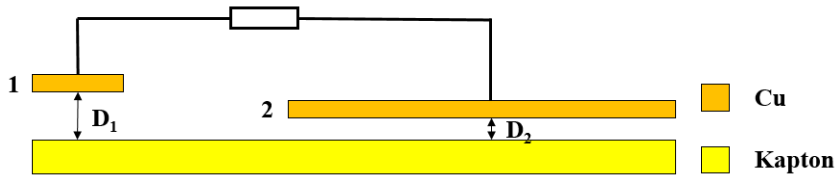

R-DC-TENG can be simplified as two plate capacitors, electrode 1 is an electrostatic breakdown electrode (EBE_1), the distance between EBE_1 and Kapton film is D_1, electrode 2 is a friction electrode (FE_2), the distance between FE_2 and Kapton film is D_2. So, according to the plate capacitance principle, the voltages V_1 & V_2 of plate

capacitors 1 and 2 can be expressed below:

$$V_1 = \frac{Q_1}{C_1},\ V_2 = \frac{Q_2}{C_2} \tag{1}$$

$$Q_1 = \sigma_1 S_1,\ Q_2 = \sigma_2 S_2 \tag{2}$$

$$C_1 = \frac{\varepsilon S_1}{4\pi k D_1},\ C_2 = \frac{\varepsilon S_2}{4\pi k D_2} \tag{3}$$

$$V_1 = \frac{\sigma_1}{\varepsilon} 4\pi k D_1,\ V_2 = \frac{\sigma_2}{\varepsilon} 4\pi k D_2 \tag{4}$$

Here,

Q_1, Q_2 are the quantities of charges on the surface of FE and EBE respectively;

C_1, C_2 are the capacitances of plate capacitors 1 and 2;

σ_1, σ_2 are the charge densities on the surfaces of EBE and FE respectively;

S_1, S_2 are the areas of EBE and FE relative to Kapton respectively;

D_1, D_2 are the gap distances between electrodes and Kapton;

ε is the permittivity;

k is the electrostatic force constant;

In the case of this paper, V_1 and V_2 are treated identically, so

$$\sigma_1 D_1 = \sigma_2 D_2 \tag{5}$$

All the charges Q_0 harvested from Kapton film distribute on the electrodes, so

$$Q_0 = Q_1 + Q_2 \tag{6}$$

$$Q_0 = \sigma_0 S = \sigma_0 l w \tag{7}$$

Here, σ is the charge density on the surface of Kapton film; l is the rotating distance, w is the effective contact width between FE and Kapton film.

From Equs. (5)-(7), we can obtain

$$\sigma_2 = \sigma l w \frac{D_1}{S_1 D_2 + S_2 D_1} \tag{8}$$

Note S2: Theoretical derivation of R-DC-TENG power generation performance at different speeds

We assume that the air breakdown Voltage is V_b, the air breakdown charge density is σ_b, and the charge density on the surface of the frictional electrode is $\sigma_b D_1 / D_2$, based on Equation (5). The quantity of charges transferred from frictional yarns to electrostatic breakdown yarns, or quantity of charges neutralized by air breakdown, can be calculated as follow:

$$Q_n = Q_0 - Q_L \tag{9}$$

Q_n is the quantity of charges transferred from FE to EBE;

Q_0 is quantity of charges collected by FE

Q_L is quantity of charges left on the electrode

When the rotor speed is 50 r/min, 100 r/min, 200 r/min, 300 r/min and the number of FEs is five, the rotation distance of the Kapton film relative to the FE in a unit time has the following relationship：

$$(1/6)l_{300} = (1/4)l_{200} = (1/2)l_{100} = l_{50} \tag{10}$$

Because the electrode width is the same, the relationship between the area of the electrode and the Kapton per unit time is as follows:

$$(1/6)S_{300} = (1/4)S_{200} = (1/2)S_{100} = S_{50} \quad (11)$$

Therefore,

$$Q_{50}=Q_{050}-Q_L=\sigma_0\ S_{50}-\sigma_b(S_1+\frac{D_2}{D_1}S_2) \quad (12)$$

$$Q_{100}=2\sigma_0\ S_{50}-2\sigma_b(S_1+\frac{D_2}{D_1}S_2)=2Q_{50} \quad (13)$$

$$Q_{200}=4\sigma_0\ S_{50}-4\sigma_b(S_1+\frac{D_2}{D_1}S_2)=4Q_{50} \quad (14)$$

$$Q_{300}=6\sigma_0\ S_{50}-6\sigma_b(S_1+\frac{D_2}{D_1}S_2)=6Q_{50} \quad (15)$$

So $Q_{300}>Q_{200}>Q_{100}>Q_{50}$,

According to Equ.(4) and Equ.(8), $V_{300}>V_{200}>V_{100}>V_{50}$. The air breakdown current will increase with the increase of speed. That is, $I_{300}> I_{200}> I_{100}>I_{50}$.

Note S3: Theoretical derivation of power generation performance of R-DC-TENG under different effective contact areas of friction electrodes.

When the rotor speed is 300 r/min and the number of FEs is 1, 2, 3, the quantity of charges transferred from FE to EBE is Q_a, Q_b, Q_C

$$Q_a=\sigma_0(S_1+S_2)-(\sigma_b S_1+\sigma_b\frac{D_2}{D_1}S_2)= S_1(\sigma_0-\sigma_b)- S_2(\sigma_0-\sigma_b\frac{D_2}{D_1}) \quad (16)$$

$$Q_b=\sigma_0(2S_1+S_2)-(2\sigma_b S_1+\sigma_b\frac{D_2}{D_1}S_2)= 2S_1(\sigma_0-\sigma_b)- S_2(\sigma_0-\sigma_b\frac{D_2}{D_1}) \quad (17)$$

$$Q_C=\sigma_0(3S_1+S_2)-(3\sigma_b S_1+\sigma_b\frac{D_2}{D_1}S_2)= 3S_1(\sigma_0-\sigma_b)- S_2(\sigma_0-\sigma_b\frac{D_2}{D_1}) \quad (18)$$

So $Q_c>Q_b>Q_a$

According to Equ.(4) and Equ.(8), $V_c>V_b>V_a$. The air breakdown current will increase with the increase of the numbers of FE. That is, $I_c> I_b> I_a$.

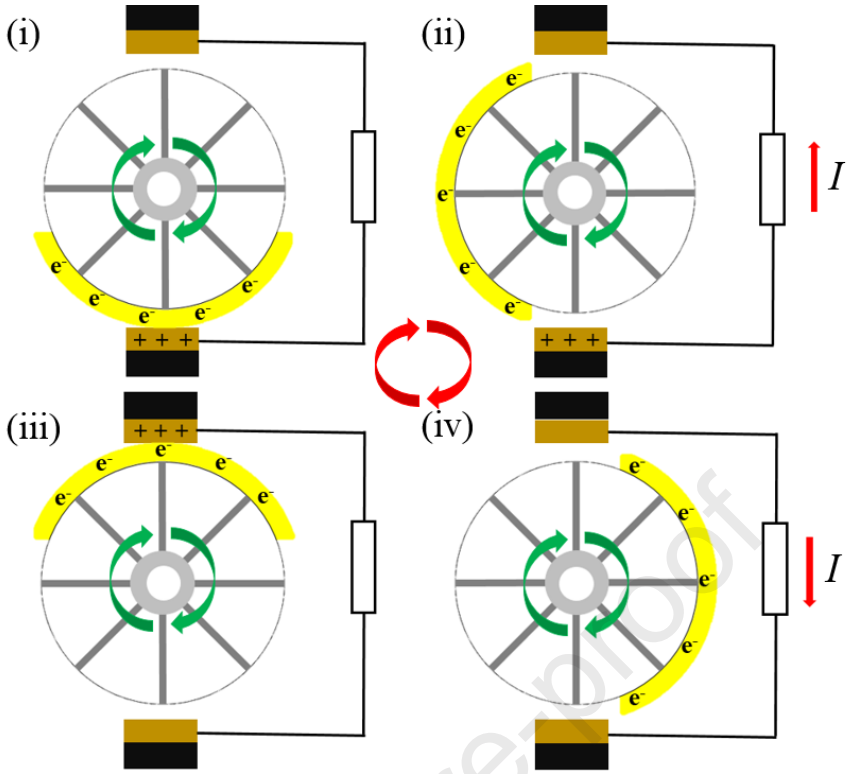

Fig. S1. Schematic of Rotary AC triboelectric nanogenerator power generation principle.

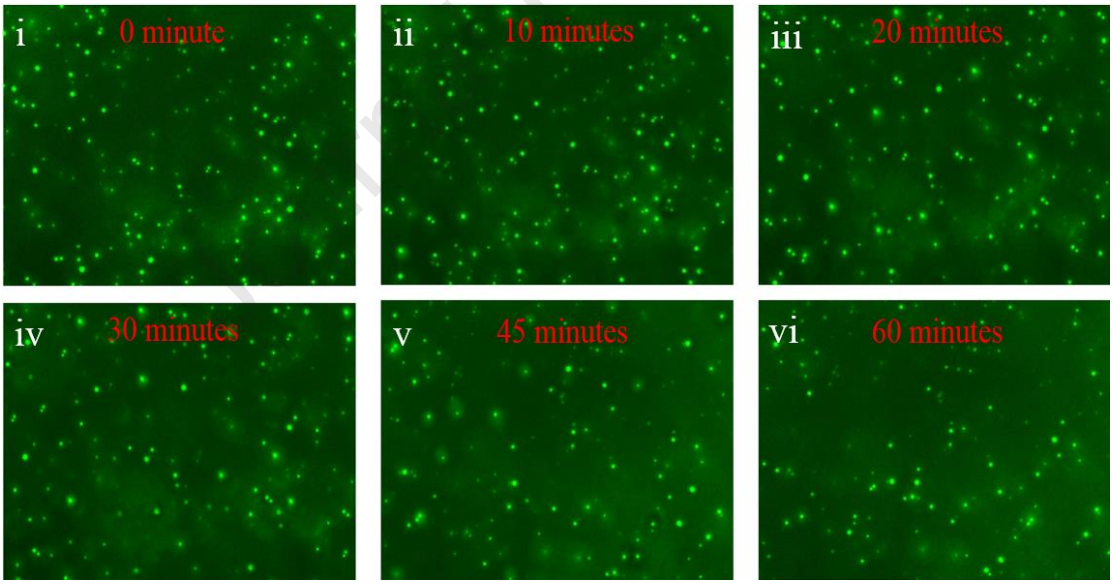

Fig. S2. Active chlorella changing in number over electrolysis time (by R-AC-TENG).

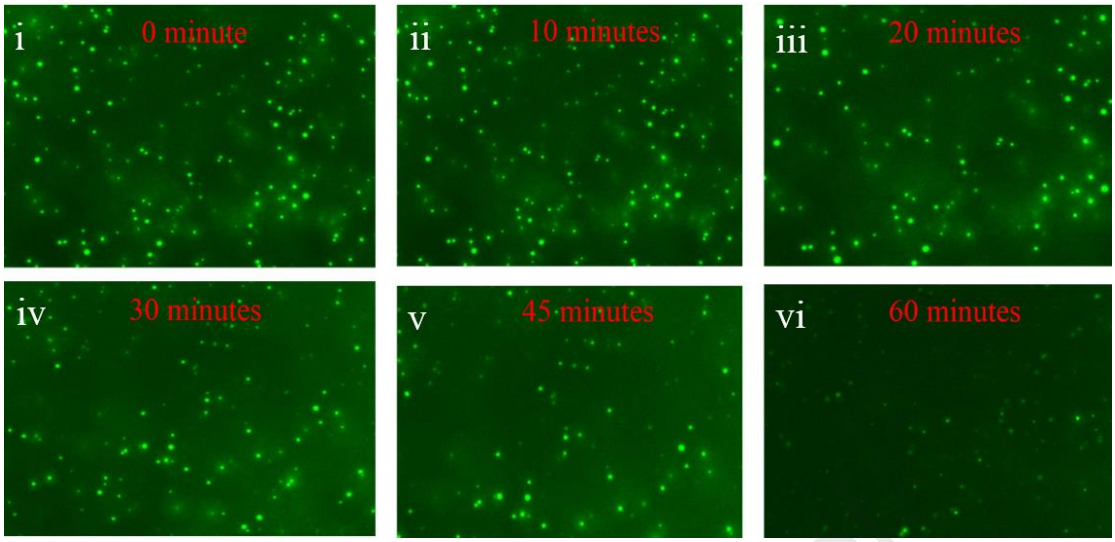

Fig. S3. Active chlorella changing in number over electrolysis time (by R-DC-TENG).

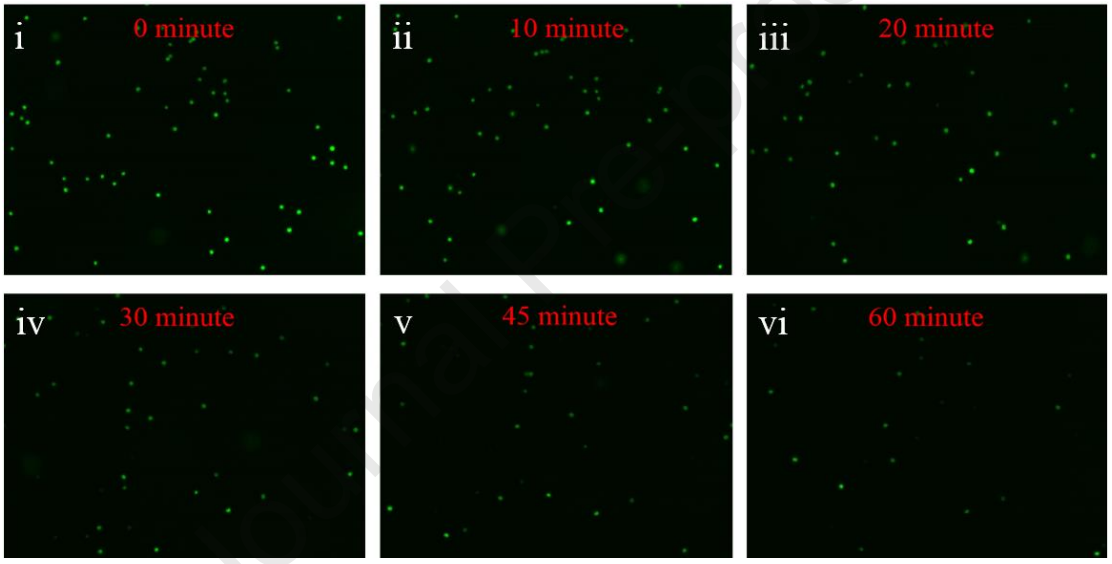

Fig. S4. Active isochrysis changing in number over electrolysis time.

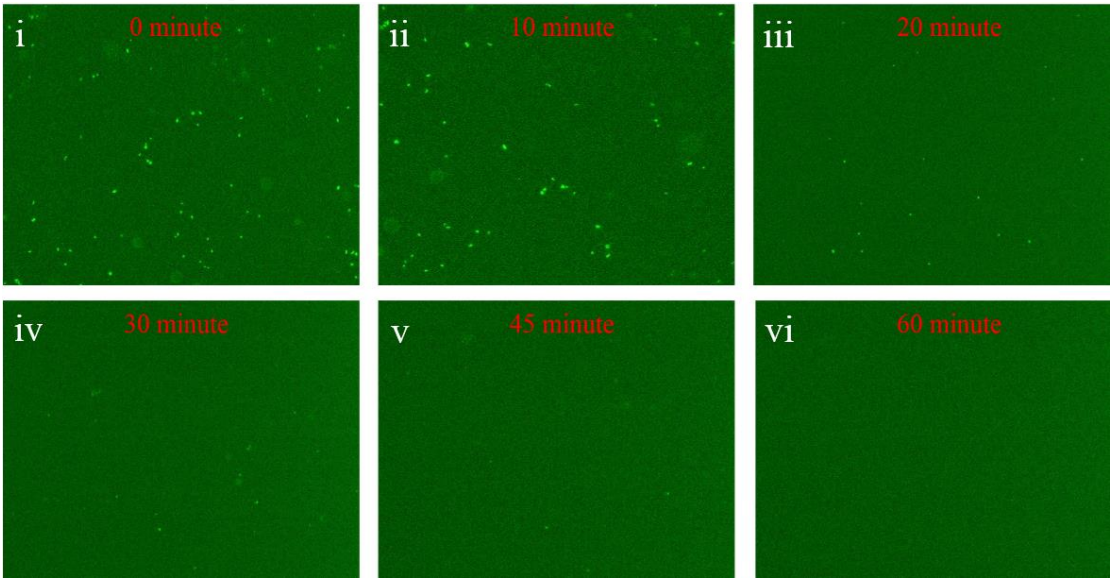

Fig. S5. Active chaetoceros changing in number over electrolysis time.

Supporting Information

A wind driven rotational direct current triboelectric nanogenerator for self-powered inactivation of seawater microorganisms

Changxin Liu[1,2*], Jianhao Liu[1,2], Jianhua Liu[1], Cong Zhao[1,2], Baichuan Shan[1,2], Nanxi Chen[1,2], Zhenghui Zhou[1,2], Chengfa Wang[1], Xinxiang Pan[3], Jianchun Mi[4], Minyi Xu[1,2]

[1]Marine Engineering College, Dalian Maritime University, Dalian, 116026, China

[2]Dalian Key Lab of Marine Micro/Nano Energy and Self-powered Systems, Marine Engineering College, Dalian Maritime University, Dalian, China

[3]School of Electronics and Information technology, Guangdong Ocean University, Zhanjiang, 524088, China

[4]College of Engineering, Peking University, Beijing, 100871, China

Files include:

Supplementary Materials and Methods

Note S1: R-DC-TENG equivalent capacitance theoretical model.

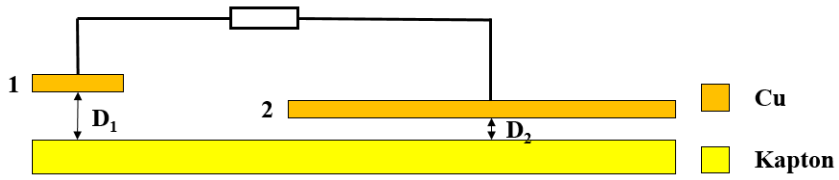

R-DC-TENG can be simplified as two plate capacitors, electrode 1 is an electrostatic breakdown electrode (EBE_1), the distance between EBE_1 and Kapton film is D_1, electrode 2 is a friction electrode (FE_2), the distance between FE_2 and Kapton film is D_2. So, according to the plate capacitance principle, the voltages V_1 & V_2 of plate

capacitors 1 and 2 can be expressed below:

$$V_1 = \frac{Q_1}{C_1},\ V_2 = \frac{Q_2}{C_2} \tag{1}$$

$$Q_1 = \sigma_1 S_1,\ Q_2 = \sigma_2 S_2 \tag{2}$$

$$C_1 = \frac{\varepsilon S_1}{4\pi k D_1},\ C_2 = \frac{\varepsilon S_2}{4\pi k D_2} \tag{3}$$

$$V_1 = \frac{\sigma_1}{\varepsilon} 4\pi k D_1,\ V_2 = \frac{\sigma_2}{\varepsilon} 4\pi k D_2 \tag{4}$$

Here,

Q_1, Q_2 are the quantities of charges on the surface of FE and EBE respectively;

C_1, C_2 are the capacitances of plate capacitors 1 and 2;

σ_1, σ_2 are the charge densities on the surfaces of EBE and FE respectively;

S_1, S_2 are the areas of EBE and FE relative to Kapton respectively;

D_1, D_2 are the gap distances between electrodes and Kapton;

ε is the permittivity;

k is the electrostatic force constant;

In the case of this paper, V_1 and V_2 are treated identically, so

$$\sigma_1 D_1 = \sigma_2 D_2 \tag{5}$$

All the charges Q_0 harvested from Kapton film distribute on the electrodes, so

$$Q_0 = Q_1 + Q_2 \tag{6}$$

$$Q_0 = \sigma_0 S = \sigma_0 l w \tag{7}$$

Here, σ is the charge density on the surface of Kapton film; l is the rotating distance, w is the effective contact width between FE and Kapton film.

From Equs. (5)-(7), we can obtain

$$\sigma_2 = \sigma l w \frac{D_1}{S_1 D_2 + S_2 D_1} \tag{8}$$

Note S2: Theoretical derivation of R-DC-TENG power generation performance at different speeds

We assume that the air breakdown Voltage is V_b, the air breakdown charge density is σ_b, and the charge density on the surface of the frictional electrode is $\sigma_b D_1 / D_2$, based on Equation (5). The quantity of charges transferred from frictional yarns to electrostatic breakdown yarns, or quantity of charges neutralized by air breakdown, can be calculated as follow:

$$Q_n = Q_0 - Q_L \tag{9}$$

Q_n is the quantity of charges transferred from FE to EBE;

Q_0 is quantity of charges collected by FE

Q_L is quantity of charges left on the electrode

When the rotor speed is 50r/min, 100r/min, 200r/min, 300r/min and the number of FEs is five, the rotation distance of the Kapton film relative to the FE in a unit time has the following relationship：

$$(1/6) l_{300} = (1/4) l_{200} = (1/2) l_{100} = l_{50} \tag{10}$$

Because the electrode width is the same, the relationship between the area of the electrode and the Kapton per unit time is as follows:

$$(1/6)S_{300} = (1/4)S_{200} = (1/2)S_{100} = S_{50} \quad (11)$$

Therefore,

$$Q_{50}=Q_{050}-Q_L=\sigma_0\ S_{50}-\sigma_b(S_1+\frac{D_2}{D_1}S_2) \quad (12)$$

$$Q_{100}=2\sigma_0\ S_{50}-2\sigma_b(S_1+\frac{D_2}{D_1}S_2)=2Q_{50} \quad (13)$$

$$Q_{200}=4\sigma_0\ S_{50}-4\sigma_b(S_1+\frac{D_2}{D_1}S_2)=4Q_{50} \quad (14)$$

$$Q_{300}=6\sigma_0\ S_{50}-6\sigma_b(S_1+\frac{D_2}{D_1}S_2)=6Q_{50} \quad (15)$$

So $Q_{300}>Q_{200}>Q_{100}>Q_{50}$,

According to Equ.(4) and Equ.(8), $V_{300}>V_{200}>V_{100}>V_{50}$. The air breakdown current will increase with the increase of speed. That is, $I_{300}> I_{200}> I_{100}>I_{50}$.

Note S3: Theoretical derivation of power generation performance of R-DC-TENG under different effective contact areas of friction electrodes.

When the rotor speed is 300r/min and the number of FEs is 1, 2, 3, the quantity of charges transferred from FE to EBE is Q_a, Q_b, Q_C

$$Q_a=\sigma_0(S_1+S_2)-(\sigma_b S_1+\sigma_b\frac{D_2}{D_1}S_2)= S_1(\sigma_0-\sigma_b)- S_2(\sigma_0-\sigma_b\frac{D_2}{D_1}) \quad (16)$$

$$Q_b=\sigma_0(2S_1+S_2)-(2\sigma_b S_1+\sigma_b\frac{D_2}{D_1}S_2)= 2S_1(\sigma_0-\sigma_b)- S_2(\sigma_0-\sigma_b\frac{D_2}{D_1}) \quad (17)$$

$$Q_C=\sigma_0(3S_1+S_2)-(3\sigma_b S_1+\sigma_b\frac{D_2}{D_1}S_2)= 3S_1(\sigma_0-\sigma_b)- S_2(\sigma_0-\sigma_b\frac{D_2}{D_1}) \quad (18)$$

So $Q_c>Q_b>Q_a$

According to Equ.(4) and Equ.(8), $V_c>V_b>V_a$. The air breakdown current will increase with the increase of the numbers of FE. That is, $I_c> I_b> I_a$.

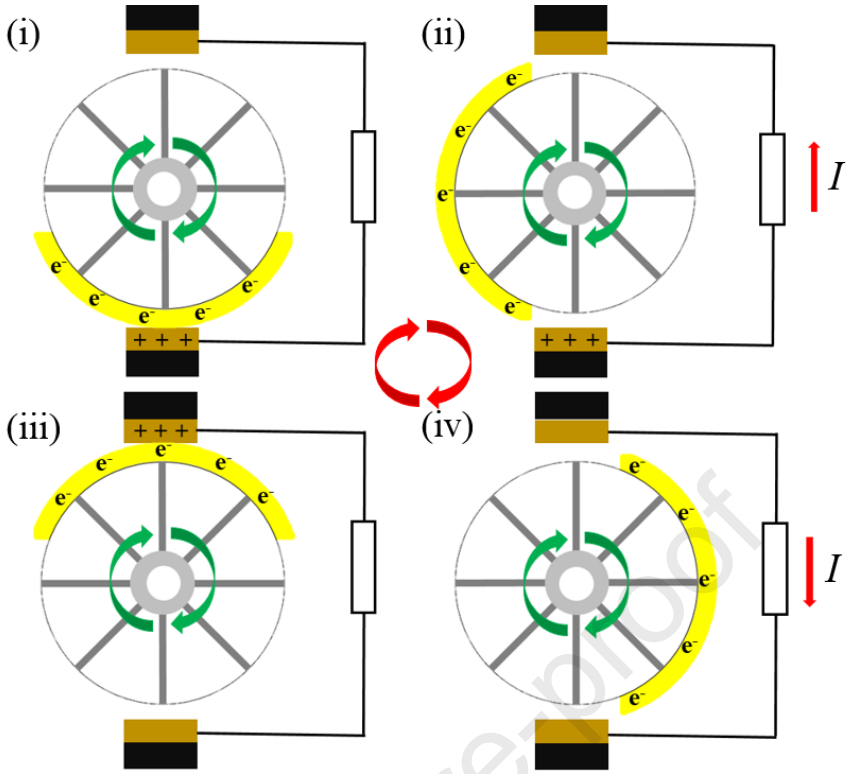

Fig. S1. Schematic of Rotary AC triboelectric nanogenerator power generation principle.

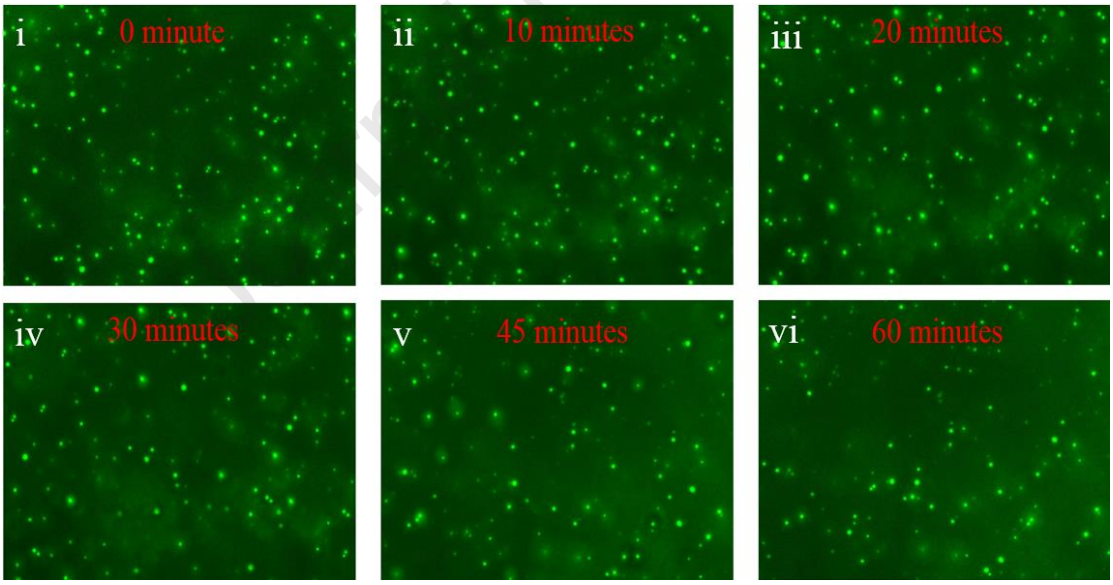

Fig. S2. Active chlorella changing in number over electrolysis time (by R-AC-TENG).

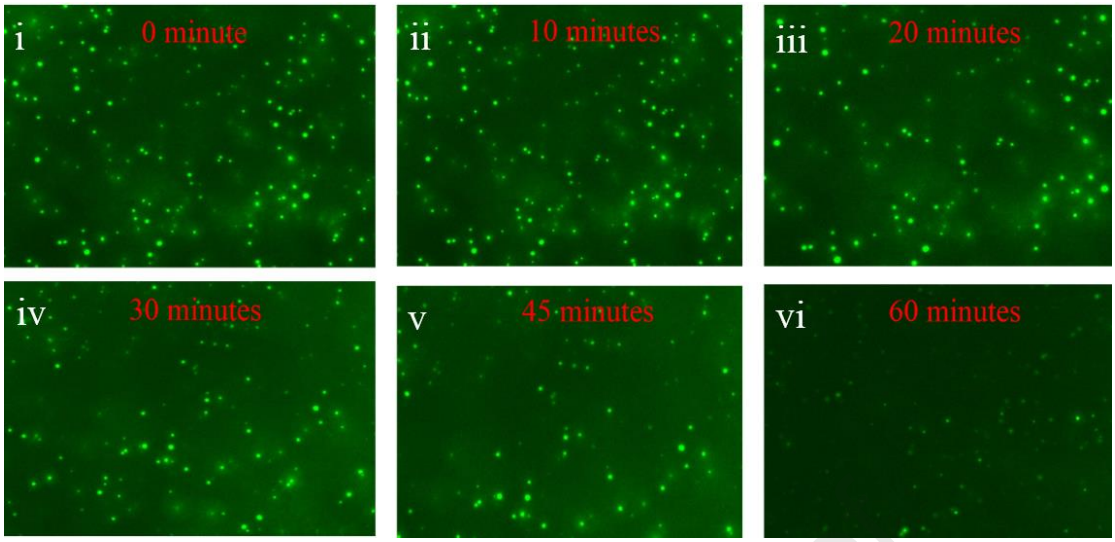

Fig. S3. Active chlorella changing in number over electrolysis time (by R-DC-TENG).

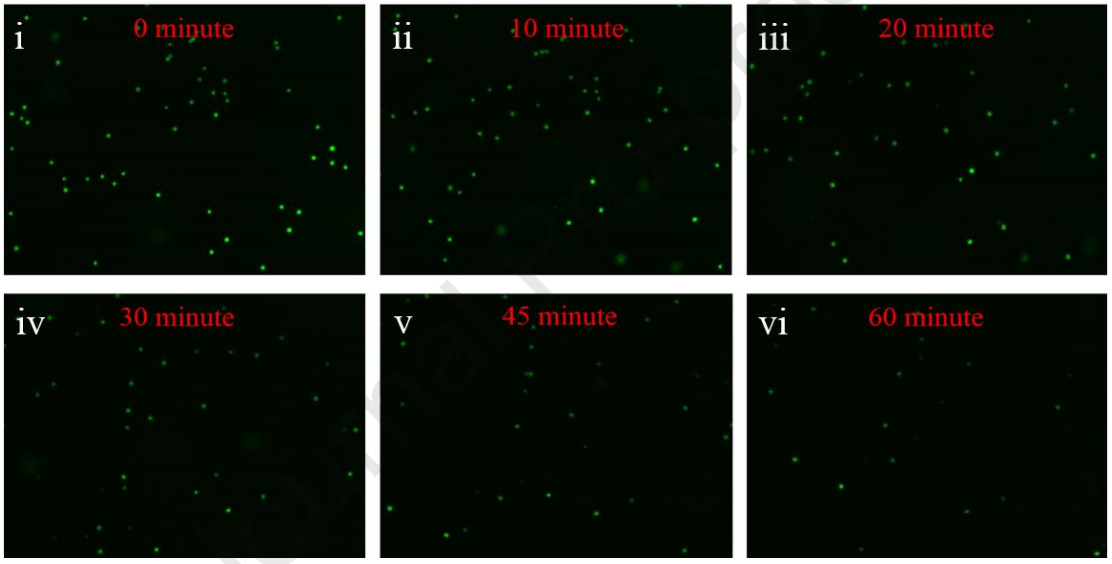

Fig. S4. Active isochrysis changing in number over electrolysis time.

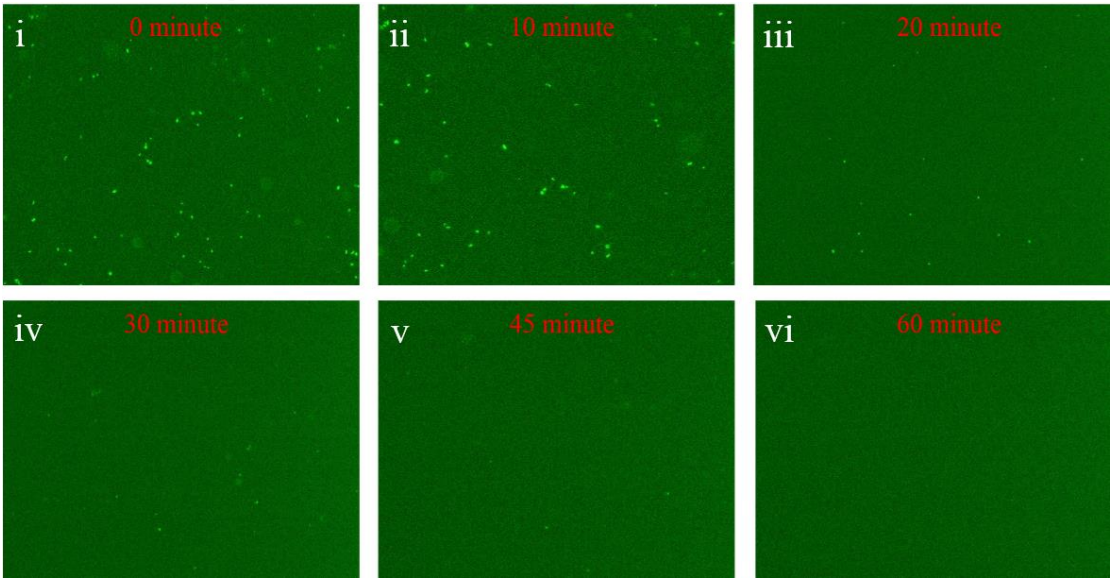

Fig. S5. Active chaetoceros changing in number over electrolysis time.

Highlights

1) A new type rotating Direct-Current triboelectric nanogenerator (R-DC-TENG) is proposed.
2) The R-DC-TENG can be as a power source and directly light up LED lights.
3) The R-DC-TENG can convert wind energy in the environment into electric energy for self-powered electrolysis of seawater to inactivate harmful marine microorganisms.

Declaration of interests

☒ The authors declare that they have no known competing financial interests or personal relationships that could have appeared to influence the work reported in this paper.

☐The authors declare the following financial interests/personal relationships which may be considered as potential competing interests: